

TiO₂-PHOTOCATALYZED DEGRADATION OF PHENOL IN SALINE MEDIA IN AN ANNULAR REACTOR: HYDRODYNAMICS, LUMPED KINETICS, INTERMEDIATES, AND ACUTE TOXICITY

E. B. Azevedo¹, A. R. Tôrres², F. R. Aquino Neto³ and M. Dezotti^{4*}

¹Department of Chemistry and Molecular Physics, Instituto de Química de São Carlos, Universidade de São Paulo (USP), Phone: + (55) (16) 3373-9962, Fax: + (55) (16)3373-9975, Av. Trabalhador São-Carlense 400, Centro, P.O. Box: 780, 13560-970, São Carlos - SP, Brazil. E-mail: bessa@iqsc.usp.br

²Chemistry and Environment Department, Faculdade de Tecnologia, Universidade do Estado do Rio de Janeiro (UERJ), Phone: + (55) (24) 3354-0194, Fax: + (55) (24) 3354-7875, Estrada Resende-Riachuelo s/n, 27523-000, Morada da Colina, Resende - RJ, Brazil. E-mail: artorres@fat.uerj.br

³LADETEC, Organic Chemistry Department, Instituto de Química, Universidade Federal do Rio de Janeiro (UFRJ) Phone: + (55) (21) 2562-7134, Fax: + (55) (21) 2260-3967, Centro de Tecnologia, Bloco A, Sala 607, 21945-970, Rio de Janeiro - RJ, Brazil. E-mail: radler@iq.ufrj.br

⁴Water Pollution Control Lab, Programa de Engenharia Química, COPPE, Universidade Federal do Rio de Janeiro (UFRJ), Centro de Tecnologia, Phone: + (55) (21) 2562-8347, Fax: + (55) (21) 2562-8300, Bloco G, Sala 115, P.O. Box: 68502, 21945-970, Rio de Janeiro - RJ, Brazil, E-mail: mdezotti@peq.coppe.ufrj.br

(Submitted: April 20, 2005 ; Revised: July 17, 2007 ; Accepted: July 21, 2007)

Abstract - The photocatalytic degradation of phenol in aqueous suspensions of TiO₂ under different salt concentrations in an annular reactor has been investigated. In all cases, complete removal of phenol and mineralization degrees above 90% were achieved. The reactor operational parameters were optimized and its hydrodynamics characterized in order to couple mass balance equations with kinetic ones. The photodegradation of the organics followed a Langmuir-Hinshelwood-Hougen-Watson lumped kinetics. From GC/MS analyses, several intermediates formed during oxidation have been identified. The main ones were catechol, hydroquinone, and 3-phenyl-2-propenal, in this order. The formation of negligible concentrations of 4-chlorophenol was observed only in high salinity medium. Acute toxicity was determined by using *Artemia sp.* as the test organism, which indicated that intermediate products were all less toxic than phenol and a significant abatement of the overall toxicity was accomplished, regardless of the salt concentration.

Keywords: Photocatalysis; TiO₂; Phenol; Saline; Intermediate; Toxicity.

INTRODUCTION

Heterogeneous photocatalysis is an advanced oxidation process (AOP), which generates hydroxyl radicals ([•]OH) by oxidation of adsorbed OH⁻ or H₂O molecules on a semiconductor surface while it is irradiated with light of energy greater than its band gap

(Linsebigler et al., 1995). The [•]OH radicals are extremely powerful oxidants, being able to degrade a great variety of organic compounds (Herrmann, 1999).

A semiconductor suited for photocatalysis has to be (i) photoactive, (ii) able to use visible or near-UV light, (iii) biologically and chemically inert, (iv) photostable, and (v) supplied at a reasonable low

*To whom correspondence should be addressed

cost (Mills and Davies, 1993). Of all known semiconductors, titanium dioxide (TiO_2) is the one that fulfills almost all the previous conditions, except for the fact that it absorbs only in the UV region.

Photocatalysis (TiO_2/UV) is a fast growing field of basic and applied research, especially due to its application in effluent decontamination (Torres et al., 2007, Santos et al., 2006, Litter, 1999, Hoffmann et al., 1995).

Phenols are used in many kinds of industries, such as paper mills, herbicide and fungicide production, etc. (Baird, 1998). Phenols and their degradation products (polyphenols, quinones, etc.) in the environment are major aquatic pollutants because they are quite toxic. Besides that, as they are relatively stable and soluble in water, their degradation to reach present safety levels in the range of $0.1 - 1.0 \text{ mg L}^{-1}$ is not an easy task.

Photocatalysis has been proven to be a plausible technique to decontaminate phenolic wastewaters as complete mineralization has been successfully achieved under a variety of conditions (Serpone et al., 1993, D'Oliveira, 1990). However, few papers have addressed the efficiency of this novel technology in saline media (Bessa et al., 1999, Bessa et al., 2001, Al-Rasheed and Cardin, 2003). This knowledge becomes fundamental as the increasing demand of water is leading to its intensive reuse and recycling, which generates the build-up of salts, making it necessary to assess the performance of photocatalysis in saline environments.

Therefore, this paper investigates the performance of photocatalysis using a TiO_2 slurry in an annular reactor with closed recycle, at three levels of salinity: 0, 2 and 50 g L^{-1} of sodium chloride (representative of reuse and marine waters, respectively). The results in terms of phenol removal, organics mineralization, intermediates produced and their respective acute toxicity were compared to the ones achieved in the absence of salt.

Also, the reactor hydrodynamics and the lumped kinetics of the degradation process were determined. In a previous work (Azevedo et al., 2004), our group studied the same chemical system with one main difference: a CSTR (Continuous Stirred Tank Reactor) operated in batch mode was used. In fact, these two systems represent the extremes of the possible configurations that can be used (Levenspiel, 1987).

MATERIALS AND METHODS

Reagents

All chemicals used were at least reagent grade and were used as received, except for phenol, which was distilled under reduced pressure and the middle fraction collected for the experiments. TiO_2 (Degussa P25, 30 nm particle size, and $50 \pm 15 \text{ m}^2 \text{ g}^{-1}$ BET surface area) was used. Solutions were prepared with distilled water.

Photocatalytic Experiments

Experiments were carried out in the apparatus shown in Figure 1. The annular reactor (inner tube made of quartz) was supplied by UMEX (model MINI Plus 4 AA 45 G). It uses a 4 W germicidal lamp as the UV-light source (radiant flux of $25 \text{ mJ} \cdot \text{m}^{-2} \cdot \text{s}^{-1}$ at $\lambda = 253.7 \text{ nm}$). The system total volume was 6.0 L (5.98 L for the mixture tank, pump, and connections plus 0.186 L for the photocatalytic reactor). A 100 mg L^{-1} phenol solution at $\text{pH} = 7.0$ was used. All experiments were performed at $25 \pm 1^\circ\text{C}$. Three sodium chloride concentrations were tested: 0, 2, and 50 g L^{-1} . In order to remove photocatalyst particles before analyses, samples were filtered through $0.45 \mu\text{m}$ pore size cellulose acetate filters.

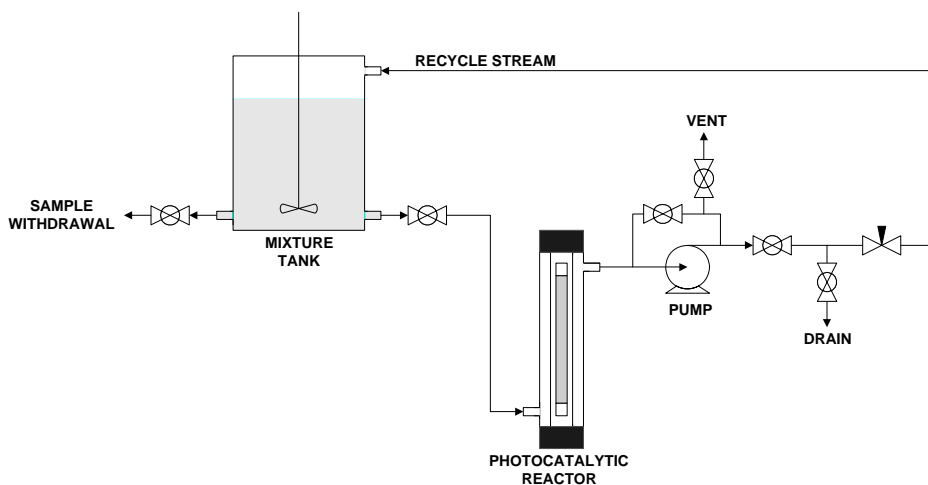


Figure 1: Scheme of the batch photocatalytic annular reactor with recycle.

Photocatalytic Reactor Optimization

In order to determine the best photocatalyst (TiO₂) concentration and flow rate, a central composite design was performed with 5 repetitions of the central point, to which were later added 3 experiments with a higher TiO₂ concentration (Montgomery, 1991). Concentrations (C) of 0.5, 1.5, 2.5, and 3.5 g L⁻¹ and flow rates (Q) of 30, 60, and 90 L h⁻¹ were tested. Normalized concentrations (x₁) and flow rates (x₂) were calculated with Equations 1 and 2, respectively. Two response factors were used: the remaining Dissolved Organic Carbon (DOC) and the absorbance at the λ_{max} for phenol (269.5 nm). In all experiments, the irradiation time was 24 hours.

$$x_1 = \frac{C - 1.5}{1.0} \quad (1)$$

$$x_2 = \frac{Q - 60}{30} \quad (2)$$

Analyses

Samples were irradiated until the phenol concentration was decreased to less than 0.5 mg L⁻¹ and a mineralization of approximately 90% was accomplished. Those criteria were followed by measuring the absorbance at 269.5 nm with a Shimadzu UV-160A spectrophotometer and Dissolved Organic Carbon (DOC) with a Shimadzu TOC-5000A Carbon Analyzer.

Chromatographic analyses were performed in order to specifically determine phenol degradation and identify the intermediates produced. Prior to chromatography, samples were submitted to a liquid-liquid extraction procedure using dichloromethane as the solvent (Goldberg and Weiner, 1980, Czuczwa et al., 1987, Azevedo, 2003).

For determining the remaining phenol concentration after irradiation, a Shimadzu GC-17A gas chromatograph provided with a DB-5 (30 m × 0.25 mm × 0.25 μm) column and a FID detector was employed. The GC was temperature programmed: the injection and detector ports were held at 250 and 280°C, respectively, and the GC oven started at 75°C and increased to 250°C at 10°C min⁻¹. The column head pressure was also programmed: it started at 40 kPa and was increased to 70 kPa at 1.7 kPa min⁻¹. The carrier gas (H₂) was then kept at a flow rate of 0.80 mL min⁻¹ and a linear speed of 25 cm s⁻¹. 1.0 μL of the extract was injected in split mode (1:30).

The samples used for identifying the intermediate products formed in the course of photocatalysis were derivatized with N,O-bis(trimethylsilyl) trifluoroacetamide (BSTFA). The analyses were performed in a 5890 Series II Hewlett Packard gas chromatograph coupled with a 5972 Hewlett Packard mass spectrometer in scan mode between 40 and 400 m/z. The same DB-5 column and temperature program described previously were used. The column head pressure was kept at 41 kPa. The carrier gas (He) flow rate and linear speed were 0.86 mL min⁻¹ and 34 cm s⁻¹, respectively. 2.0 μL of the derivatized extract were injected in splitless mode.

Toxicity assays were carried out according to Petrobras standards N-2588 and N-2594 (Petrobras, 1996a, Petrobras, 1996b) using *Artemia sp.* as the test organism. Statistical analyses performed to determine the LC₅₀ parameter were based on the adjusted Spearman-Kärber method (Hamilton et al., 1977).

Mass balance and reaction rate equations were integrated by an explicit method for stiff problems (Runge-Kutta type) where the Jacobian matrix was provided. Kinetic and adsorption constants were estimated by a least squares regression quasi-Newtonian algorithm (Chapra and Canale, 1998).

RESULTS AND DISCUSSION

Control Experiments

Control experiments with no photocatalyst (photolysis only) and in the absence of irradiation (adsorption only) were performed, showing no significant phenol degradation or loss during the periods of time used. Figure 2 depicts those findings.

Photocatalytic Reactor Optimization

Figure 3 shows the contour plots that are the projections of the response surfaces obtained from the experimental design in the flow rate × TiO₂ concentration (Q × C_{TiO₂}) plane. On both surfaces an incomplete cubic model was fitted.

For Figure 3a, the DOC surface determination coefficient (R²) was 1.00. The minimum (higher degradation) is at Q ≅ 54 L h⁻¹ and C_{TiO₂} ≅ 2.2 g L⁻¹. For Figure 3b, the phenols absorbance surface R² was 0.998 with a minimum at Q ≅ 60 L h⁻¹ and C_{TiO₂} ≅ 2.4 g L⁻¹. Therefore, the average values were chosen to be used in the photocatalytic experiments, that is, Q = 57 L h⁻¹ and C_{TiO₂} = 2.3 g L⁻¹.

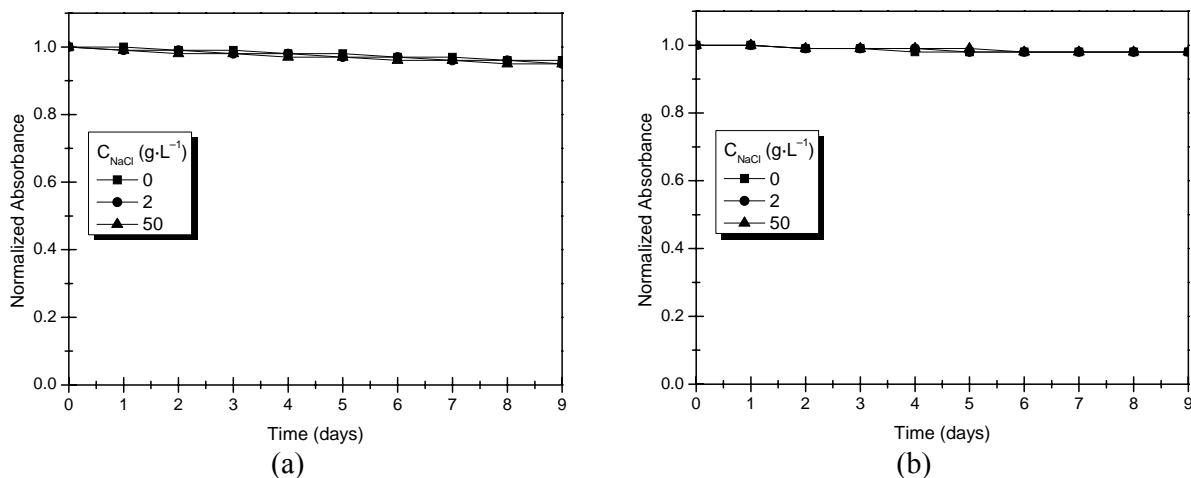


Figure 2: Control experiments performed: (a) photolysis and (b) adsorption.

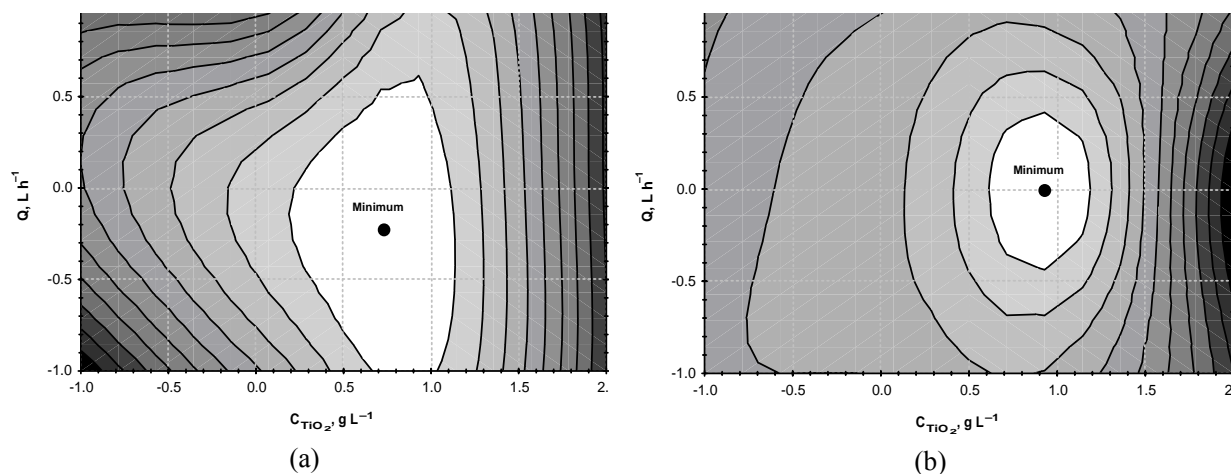


Figure 3: Contour plots for the photocatalytic reactor optimization. Normalized response factors: (a) Dissolved Organic Carbon (DOC) in $\text{mg}\cdot\text{L}^{-1}$ and (b) Phenol peak absorbance ($\lambda_{\text{max}} = 269.5 \text{ nm}$).

Photocatalytic Reactor Hydrodynamics Characterization

Ideally, the mixture tank would be a Continuous-Stirred-Tank Reactor (CSTR) with a high degree of agitation. On the other hand, the photocatalytic reactor, due to the lack of agitation and to the downstream position of the pump, would be a Plug-and-Flow Reactor (PFR). However, deviations from ideality are common and should be accounted for in the kinetic models.

Therefore, in accordance with several authors (Smith, 1981, Levenspiel, 1987, Fogler, 1999), the step perturbation methodology and the Agitated Tanks in Series model was used to fit the data. The tracer was potassium permanganate (KMnO_4) and the measured variable was the absorbance at the λ_{max} for permanganate (525 nm) in the exit stream.

It can be demonstrated that the relation between $J(\theta)$ and n is given by Equation 3:

$$J_n(\theta) = \left(\frac{A_n}{A_0} \right)_{\text{step}} = 1 - e^{-\frac{n\theta}{\theta_m}} \left[1 + \frac{n\theta}{\theta_m} + \frac{1}{2!} \left(\frac{n\theta}{\theta_m} \right)^2 + \dots + \frac{1}{(n-1)!} \left(\frac{n\theta}{\theta_m} \right)^{n-1} \right] \quad (3)$$

where: θ is the hydraulic residence time; $J_n(\theta)$ is the hydraulic residence time distribution function, which is the fraction of the effluent stream that has a residence time less than θ ; n is the number of CSTRs in series; A_n is the tracer absorbance; A_0 is the tracer initial absorbance; and θ_m is the average hydraulic residence time for each tank.

A particular case of this expansion in series is when $n=1$, a situation in which the response curve for one CSTR is obtained, as depicted in Equation 4:

$$J_n(\theta) = \left(\frac{A_n}{A_0} \right)_{\text{step}} = 1 - e^{-\frac{\theta}{\theta_m}} \quad (4)$$

Figure 4 shows the results obtained in the characterization studies. For the mixture tank, it can be seen that the agreement between the experimental data and the curve for one tank was excellent, corresponding to a determination coefficient of 0.999. However, for the photocatalytic reactor, the experimental data sometimes agree with the $n=3$ curve, sometimes with the $n=5$ one. Therefore, to correct this discrepancy, the reactor was substituted by four CSTRs in series, corresponding to an average value for n , since the experimental data agree partly with $n=3$, and partly with the $n=5$ curves.

It is noteworthy that the experimental data for the photocatalytic reactor do not fit precisely to any curve. This is a common event due to other non-idealities, such as: “dead” volumes, bypassing, channeling, etc., that cause deviations from the expected behavior.

UV Spectrophotometry

The absorption spectra of all samples were scanned from 200 to 330 nm in order to follow:

- a) The disappearance of the phenol peak at 269.5 nm;

- b) The mineralization progress, as the area under the UV spectrum can be regarded as a semi-quantitative measure of the concentration of conjugated unsaturated compounds; and
- c) The aromatic ring rupture by the absorption of carbonylated and carboxylated compounds between 235 and 240 nm.

Figure 5 shows the results obtained. In Figure 5a, it can be seen that phenol degradation was accomplished regardless of the presence of sodium chloride. However, by the end of the treatment time, phenol degradation in saline media was somewhat smaller.

From Figure 5b it can be observed that the amount of UV-absorbing species is increased during the course of degradation, returning to the initial level of absorbance after 45% of the total irradiation time. This is compatible with the formation and later degradation of compounds with increased conjugation (Okamoto et al., 1985, Richard and Boule, 1994, Peiró et al., 2001). However, this increase was more significant with the saline media.

Figure 5c shows that the concentration of intermediates formed during the photocatalytic degradation increased with salinity.

It is worth mentioning that the annular reactor with closed recycle configuration favors the direct conversion of phenol. On the other hand, a previous work (Azevedo et al., 2004) has shown that the CSTR with no recycle configuration favors the build up of intermediates (Smith, 1981, Levenspiel, 1987, Fogler, 1999). Therefore, the different degree of interaction between intermediates and salt leads to distinct behaviors.

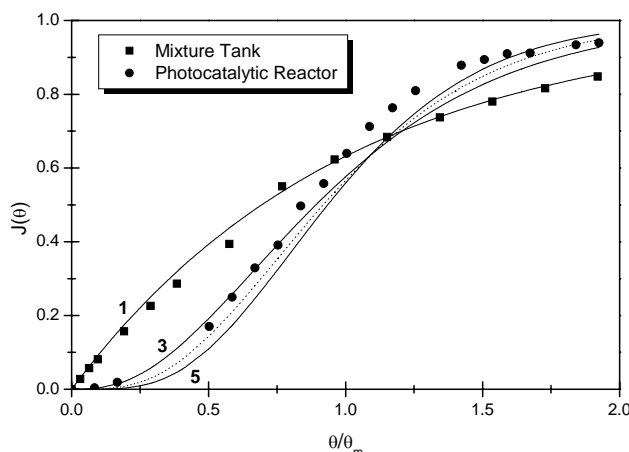


Figure 4: Results of the reactor hydrodynamics characterization. The lines are response curves for the agitated tanks in series model for 1, 3, 5 (solid), and 4 (dashed) tanks, respectively. Markers correspond to the experimental data for the mixture tank (■) and for the photocatalytic reactor (●).

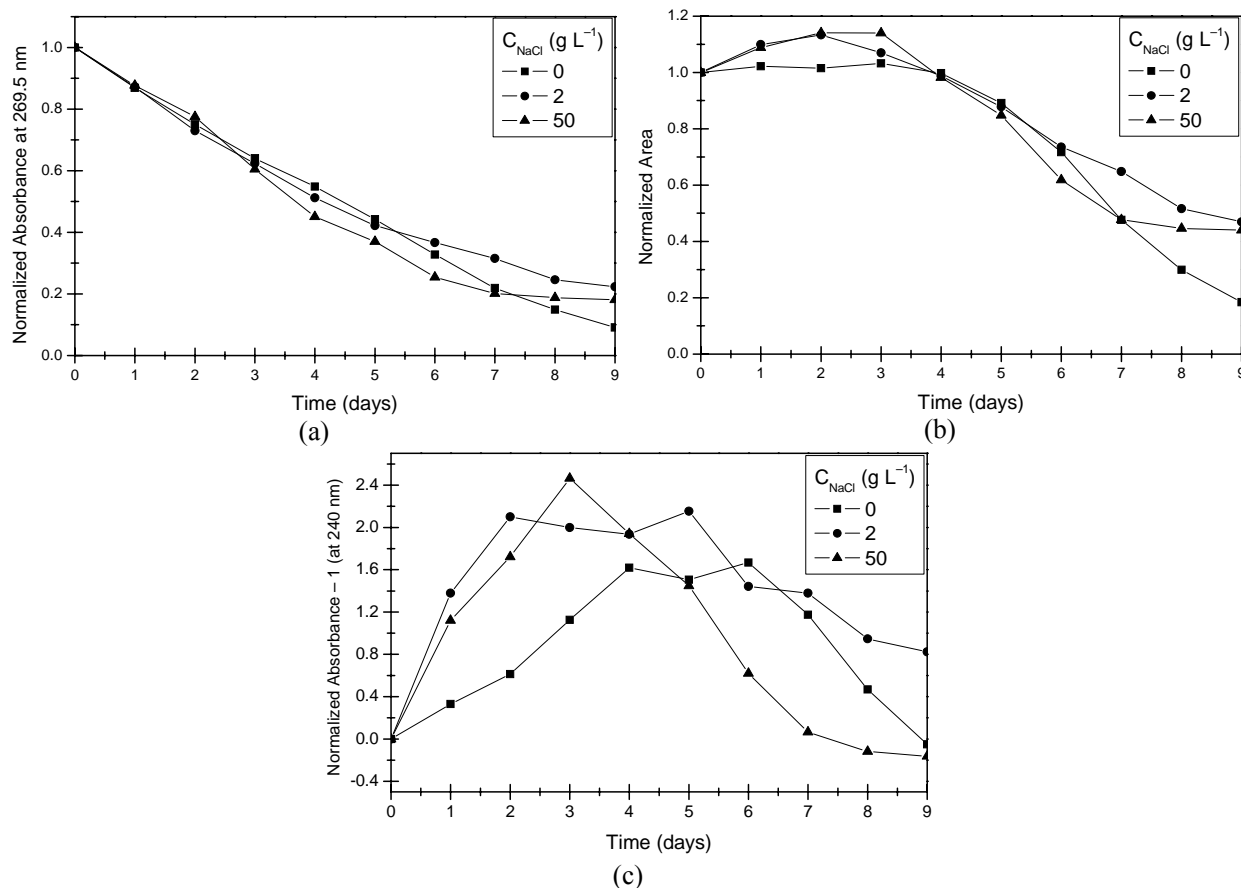


Figure 5: UV spectrophotometry: (a) Absorbance at $\lambda = 269.5$ nm (phenol peak); (b) Area under UV-absorption spectra; and (c) Absorbance at $\lambda = 240$ nm (aromatic ring rupture).

Dissolved Organic Carbon (DOC) and Gas Chromatography (GC)

DOC analyses were performed in order to evaluate the destruction of organic matter. The degrees of mineralization achieved for 0, 2, and 50 g L⁻¹ of sodium chloride were 92, 92, and 88%, respectively. As shown in Figure 6a, although there is a significant difference between the saline media and the non-saline one, by the end of the mineralization process this difference is small.

Gas chromatography was used to determine the remaining concentration of phenol. As can be observed in Figure 6b, the same pattern with respect to the salinity occurred.

Nevertheless, the results indicate that the UV-mediated photocatalysis with aerated TiO₂ suspensions of phenol can completely remove this pollutant from water and can lead to an extensive mineralization of the organic content, even in the presence of sodium chloride up to a concentration of 50 g L⁻¹.

Rate and Adsorption Constant Estimation

The estimation procedure was based on the Extended Lumped Kinetic Model (ELKM) (Belkacemi et al., 2000), which uses the Langmuir-Hinshelwood-Hougen-Watson (LHHW) approach, shown in Figure 7.

The lumps were defined as follows: Lump A: Phenol; Lump B: Intermediates; and Lump C: CO₂. Phenol concentrations, C_{At} , in mg_{Phenol} L⁻¹, determined by GC, were converted into mg_{DOC} L⁻¹ by Equation 5:

$$\text{mg}_{\text{Phenol}} \text{ L}^{-1} = \frac{72.1}{94.1} \text{mg}_{\text{DOC}} \text{ L}^{-1} \quad (5)$$

The intermediate concentrations, C_{Bt} , were determined by Equation 6:

$$C_{Bt} = \text{DOC}_0 - (C_{At} + C_{Ct}) \quad (6)$$

where DOC_0 is the initial dissolved organic carbon concentration and C_{Ct} represent the CO_2 concentrations determined by Equation 7:

$$C_{Ct} = DOC_0 - DOC_t \quad (7)$$

The reactor hydrodynamics was coupled with the model in order to adequately represent reality. Figure 8 represents the hydrodynamic model comprised of one mixture tank ($V_M = 5.8$ L) followed by four agitated tanks in series ($V_1 = V_2 = V_3 = V_4 = 4.65 \times 10^{-2}$ L).

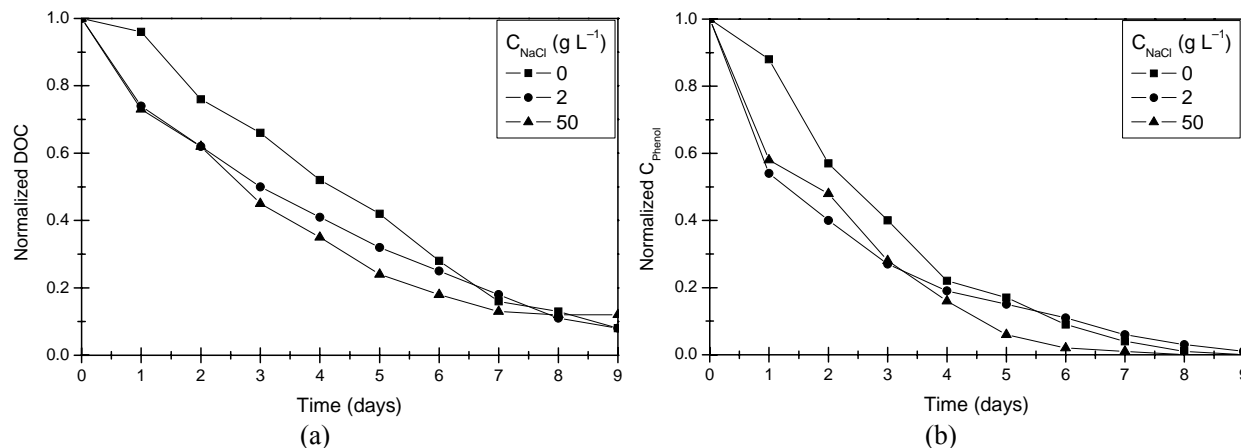


Figure 6: (a) Mineralization and (b) remaining phenol concentration vs. irradiation time.

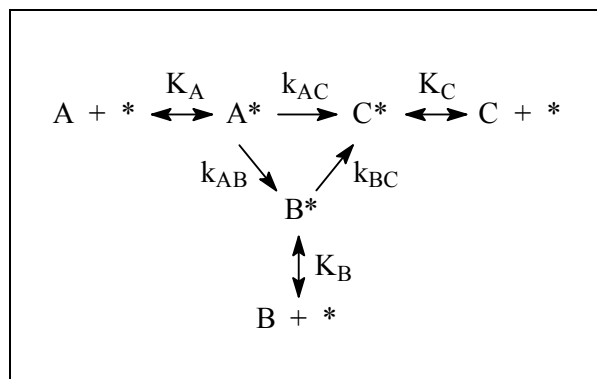


Figure 7: Extended Lumped Kinetic Model (ELKM).

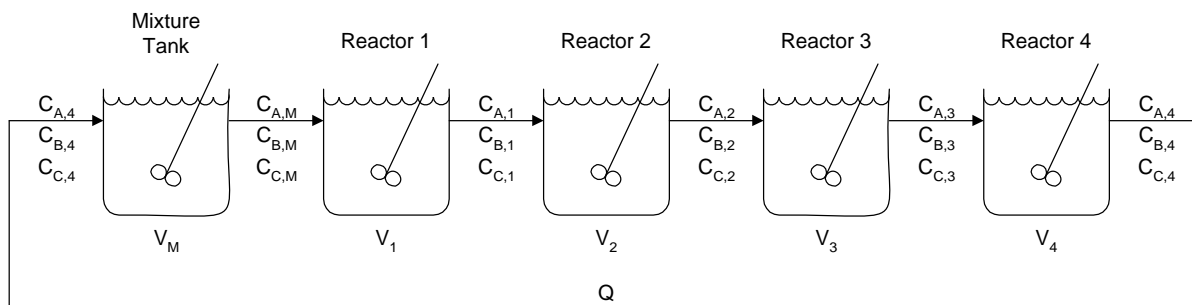


Figure 8: Scheme of the agitated-tanks-in-series model used for the reaction rate and adsorption constant estimation.

However, the ELKM model is not suitable for saline media because it does not take into consideration the fraction of the photocatalyst sites covered by chloride ion. Therefore, for saline media, an adaptation that will be referred to as the Extended Lumped Saline Kinetic Model (ELSKM) is proposed, in which a term is introduced in the denominator of the rate equations in order to account for chloride adsorption.

Thus, the ELSKM coupled with the mass balance equations derived from the reactor hydrodynamics is described by Equations 8–16, in which m_{cat} is the mass of photocatalyst inside the reactor, \tilde{k} is a reaction rate constant, and K is an adsorption constant.

Mixture Tank:

$$\frac{dC_{A,M}}{dt} = \frac{Q}{V_M} \cdot C_{A,4} - \frac{Q}{V_M} \cdot C_{A,M} \quad (8)$$

$$\frac{dC_{B,M}}{dt} = \frac{Q}{V_M} \cdot C_{B,4} - \frac{Q}{V_M} \cdot C_{B,M} \quad (9)$$

$$\frac{dC_{C,M}}{dt} = \frac{Q}{V_M} \cdot C_{C,4} - \frac{Q}{V_M} \cdot C_{C,M} \quad (10)$$

Reactor 1:

$$\frac{dC_{A,1}}{dt} = \frac{Q}{V_1} \cdot C_{A,M} - \frac{Q}{V_1} \cdot C_{A,1} - \frac{m_{\text{cat}} (\tilde{k}_{AB} + \tilde{k}_{AC}) K_A C_{A,1}}{1 + K_A C_{A,1} + K_B C_{B,1} + K_C C_{C,1} + K_{Cl^-} C_{Cl^-}} \quad (11)$$

$$\frac{dC_{B,1}}{dt} = \frac{Q}{V_1} \cdot C_{B,M} - \frac{Q}{V_1} \cdot C_{B,1} + \frac{m_{\text{cat}} (\tilde{k}_{AB} K_A C_{A,1} - \tilde{k}_{BC} K_B C_{B,1})}{1 + K_A C_{A,1} + K_B C_{B,1} + K_C C_{C,1} + K_{Cl^-} C_{Cl^-}} \quad (12)$$

$$\frac{dC_{C,1}}{dt} = \frac{Q}{V_1} \cdot C_{C,M} - \frac{Q}{V_1} \cdot C_{C,1} + \frac{m_{\text{cat}} (\tilde{k}_{AC} K_A C_{A,1} + \tilde{k}_{BC} K_B C_{B,1})}{1 + K_A C_{A,1} + K_B C_{B,1} + K_C C_{C,1} + K_{Cl^-} C_{Cl^-}} \quad (13)$$

Reactor i ($i = 2$ to 4):

$$\frac{dC_{A,i}}{dt} = \frac{Q}{V_i} \cdot C_{A,i-1} - \frac{Q}{V_i} \cdot C_{A,i} - \frac{m_{\text{cat}} (\tilde{k}_{AB} + \tilde{k}_{AC}) K_A C_{A,i}}{1 + K_A C_{A,i} + K_B C_{B,i} + K_C C_{C,i} + K_{Cl^-} C_{Cl^-}} \quad (14)$$

$$\frac{dC_{B,i}}{dt} = \frac{Q}{V_i} \cdot C_{B,i-1} - \frac{Q}{V_i} \cdot C_{B,i} + \frac{m_{\text{cat}} (\tilde{k}_{AB} K_A C_{A,i} - \tilde{k}_{BC} K_B C_{B,i})}{1 + K_A C_{A,i} + K_B C_{B,i} + K_C C_{C,i} + K_{Cl^-} C_{Cl^-}} \quad (15)$$

$$\frac{dC_{C,i}}{dt} = \frac{Q}{V_i} \cdot C_{C,i-1} - \frac{Q}{V_i} \cdot C_{C,i} + \frac{m_{\text{cat}} (\tilde{k}_{AC} K_A C_{A,i} + \tilde{k}_{BC} K_B C_{B,i})}{1 + K_A C_{A,i} + K_B C_{B,i} + K_C C_{C,i} + K_{Cl^-} C_{Cl^-}} \quad (16)$$

which are subjected to the initial conditions shown in Equations 17–21:

$$C_{A,M} = C_{A,M_0}, C_{B,M} = 0, C_{C,M} = 0 \text{ for } t = 0. \quad (17)$$

$$C_{A,1} = C_{A,1_0}, C_{B,1} = 0, C_{C,1} = 0 \text{ for } t = 0. \quad (18)$$

$$C_{A,2} = C_{A,2_0}, C_{B,2} = 0, C_{C,2} = 0 \text{ for } t = 0. \quad (19)$$

$$C_{A,3} = C_{A,3_0}, C_{B,3} = 0, C_{C,3} = 0 \text{ for } t = 0. \quad (20)$$

$$C_{A,4} = C_{A,4_0}, C_{B,4} = 0, C_{C,4} = 0 \text{ for } t = 0. \quad (21)$$

Equations 8–16 were then simultaneously integrated in time and the rate and adsorption constants estimated. Figure 9 presents the experimental data obtained (symbols) and the integrated lump distribution curves (lines).

The following considerations can be made by observing the plots in Figure 9:

a) A slight inhibition in the formation of intermediates can be observed from two kinetic parameters: t_{max} (the time needed to reach the maximum concentration of intermediates) and $C_{B,\text{max}}$ (maximum concentration of intermediates). Table 1 shows the estimated values for those parameters. It

becomes clear that $C_{B,max}$ decreases as salinity increases. The fact that t_{max} does not follow the same behavior is an indication that \tilde{k}_{AC} (the parallel reaction $A \rightarrow C$) is somewhat significant.

b) The shape of the CO₂ distribution curves at the beginning of the photocatalytic process is related to \tilde{k}_{AC} . As they do not show an initial lag phase, \tilde{k}_{AC} should indeed be significant.

The estimated values for the constants, as well as the respective determination coefficients are listed in Table 2. It is important to note that the rate constants, \tilde{k} , are apparent because they comprise the total concentration of available sites per area of TiO₂ (Belkacemi, 2000). The adsorption constants, K , are

also apparent as they were estimated for the irradiated catalyst and not in the dark.

From Table 2, the following considerations can be made:

a) The reaction rate constants increased with salinity while the adsorption ones decreased.

b) \tilde{k}_{BC} , K_A , K_B , and K_C are not significantly affected by changes in the salinity of the medium.

c) The adsorption of CO₂ on TiO₂ was not inhibited by the presence of salt.

d) The photocatalytic degradation obeys the Langmuir-Hinshelwood-Hougen-Watson approach. Therefore, lumped models like the ELKM and ELSKM used here are able to satisfactorily describe the system.

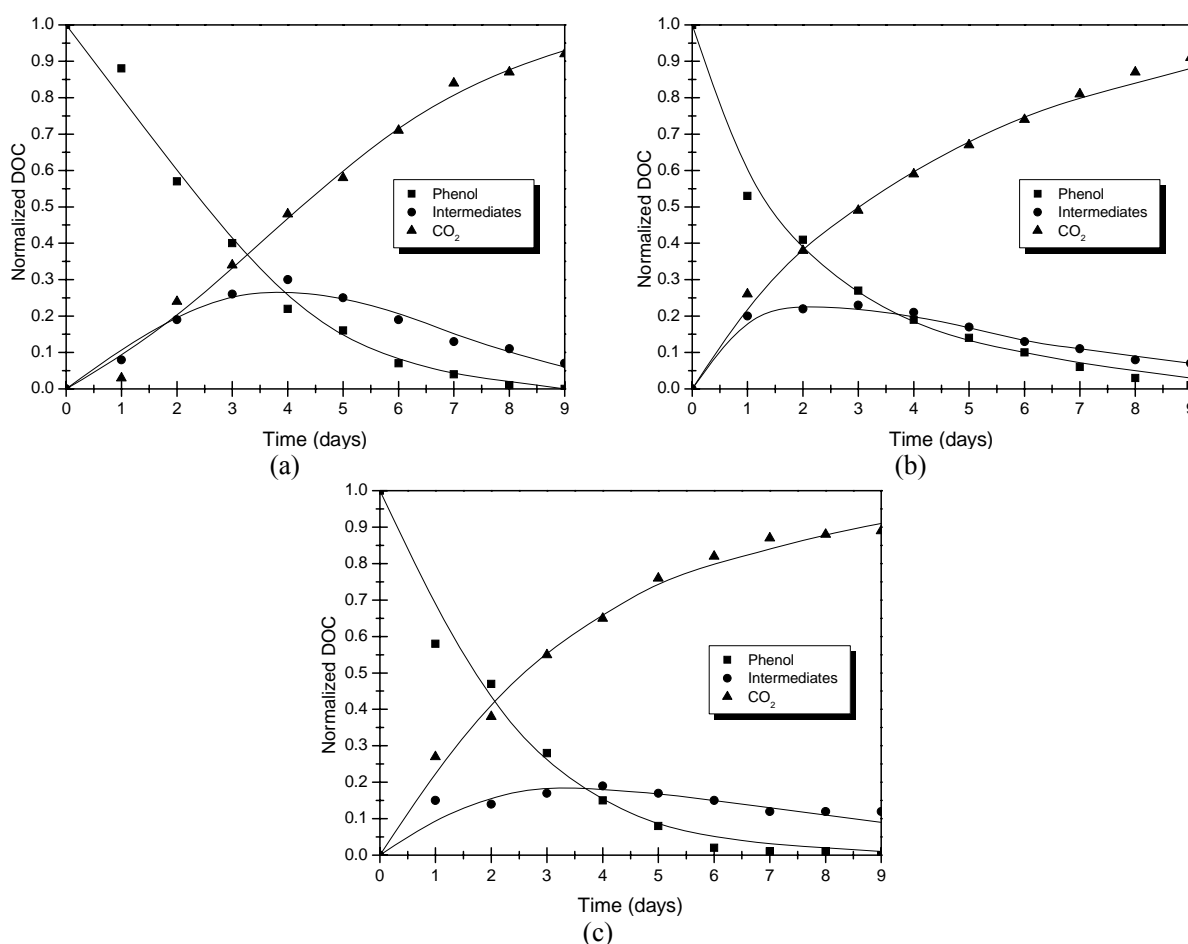


Figure 9: Lump concentration profiles: (a) 0 g L⁻¹, (b) 2 g L⁻¹, and (c) 50 g L⁻¹ of NaCl.

Table 1: t_{max} e $C_{B,max}$ observed during photocatalysis.

Kinetic Parameters	C_{NaCl} (g L ⁻¹)		
	0	2	50
t_{max} (days)	3.80	1.89	3.55
$C_{B,max}$ (mg _{DOC} L ⁻¹)	22.5	18.4	17.5

Table 2: Estimates for kinetic and adsorption constants.

Constants	C_{NaCl} (g L ⁻¹)		
	0	2	50
\tilde{k}_{AB}	5.4×10^{-3}	1.2×10^{-2}	2.3×10^{-1}
\tilde{k}_{AC}	2.8×10^{-3}	5.6×10^{-3}	4.4×10^{-1}
\tilde{k}_{BC}	1.4×10^{-3}	4.5×10^{-3}	7.1×10^{-3}
K_A	3.3×10^{-1}	2.4×10^{-1}	2.5×10^{-1}
K_B	1.7×10^0	1.0×10^0	9.5×10^{-1}
K_C	1.4×10^0	1.0×10^0	7.1×10^{-1}
K_{Cl^-}	-	5.7×10^{-4}	3.4×10^{-2}
R^2	0.990	0.999	0.997

Note: [\tilde{k}] = mg_{DOC} L⁻¹ mg_{TiO₂}⁻¹ min⁻¹; [K] = L mg_{DOC}⁻¹

Compounds Identification by GC/MS

Table 3 shows the identified compounds, the percentage of similarity between the library mass spectra and sample ones, and the respective structural formulas.

Several highly hydroxylated intermediates were detected: polyphenols, ring opening fragments, as well as compounds formed by direct coupling of phenoxy radicals and rearrangement between intermediates. Among those, four — glycerol, catechol, hydroquinone, and 4,4'-dihydroxybiphenyl — have already been reported (Okamoto et al., 1985, Augugliaro et al., 1988, Trillas et al., 1992, Richard and Boule, 1994, Alemany et al., 1997, Ilisz and Dombi, 1999, Nogueira et al., 1999, Sobczynski et al., 1999, Grimes and Ngwang, 2000, Peiró et al., 2001). The same compounds were produced regardless of the salinity, but 4-chlorophenol was formed only in the high salinity medium (50 g L⁻¹).

It should be noted that only three compounds — 3-phenyl-2-propenal, catechol, and hydroquinone —

were produced in significant amounts during the course of the photocatalytic degradation. Figure 10 shows their time distribution curves in function of salinity. It can be seen that the highest yield was for hydroquinone, followed by catechol and 3-phenyl-2-propenal. Noteworthy is also the influence of salinity. Catechol formation is severely inhibited by the presence of sodium chloride. On the contrary, 3-phenyl-2-propenal formation was significantly increased by it.

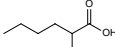
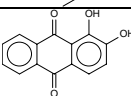
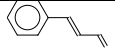
Acute Toxicity

Figure 11 shows the results obtained for the acute toxicity assays using *Artemia sp.* as the test organism.

The following considerations can be made:

- No intermediates, at the concentrations in which they were generated in the reaction mixture, presented a higher toxicity than the parent compound (phenol).
- Photocatalysis was quite efficient in removing toxicity, regardless of the concentration of salt.

Table 3: GC/MS identified intermediate compounds of phenol TiO₂/UV photocatalysis.

Compounds	Similarity*	Structural Formula	C_{NaCl} (g L ⁻¹)		
			0	2	50
2-ethylhexanol	88%		✓	✓	✓
2-furancarboxylic acid	92%		✓	✓	✓
2-ethylhexanoic acid	95%		✓	✓	✓
1,2-dihydroxy-anthraquinone	99%		✓	✓	✓
3-phenyl-2-propenal	80%		✓	✓	✓

Continuation Table 3

Compounds	Similarity*	Structural Formula	C _{NaCl} (g L ⁻¹)		
			0	2	50
4-chlorophenol	94%		nd	nd	✓
Benzoic acid	95%		✓	✓	✓
Glycerol	85%		✓	✓	✓
Catechol	94%		✓	✓	✓
Hydroquinone	93%		✓	✓	✓
Salicylic acid	96%		✓	✓	✓
α-hydroxy-2-furanacetic acid	86%		✓	✓	✓
4-(1,2-ethanediol)-catechol	90%		✓	✓	✓
4,4'-dihydroxybiphenyl	95%		✓	✓	✓

*Wiley spectral library 275; nd – not detected.

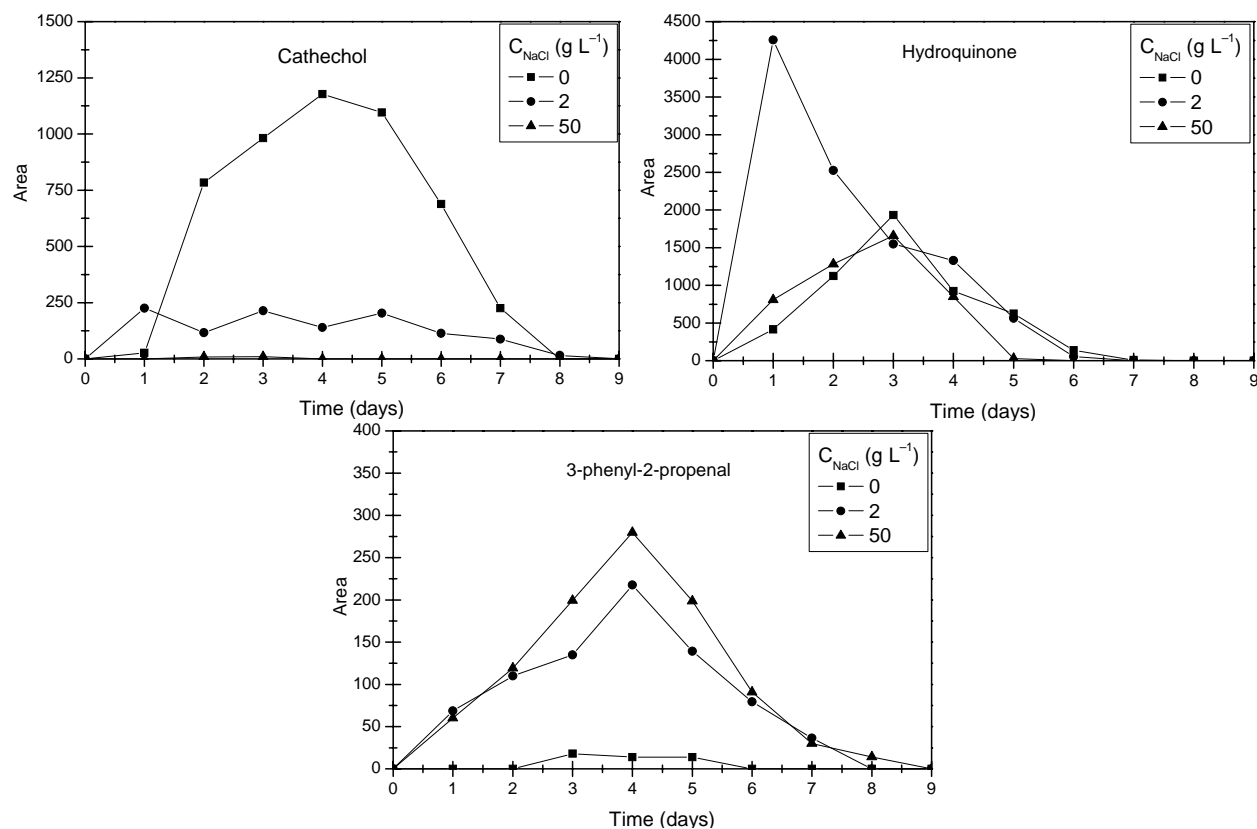


Figure 10: Plots of area (concentration) vs. irradiation time as a function of salinity for the three main intermediates identified.

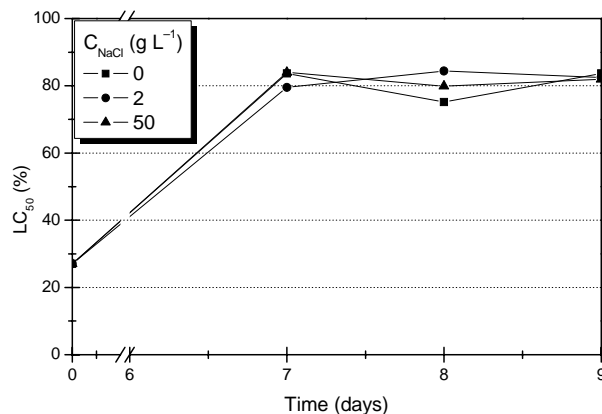


Figure 11: *Artemia sp.* LC₅₀ (%) vs. irradiation time.

CONCLUSIONS

The photocatalytic system used was capable of accomplishing phenol removal and organic matter mineralization regardless of the concentration of salt (up to 50 g L⁻¹). The study of the Residence Times Distribution (RTD) showed that the mixture tank was indeed a Continuous Stirred Tank Reactor (CSTR) and that the photocatalytic reactor could be replaced by 4 CSTRs in series.

Phenol photocatalytic degradation followed the Langmuir-Hinshelwood-Hougen-Watson model and the lumps approach greatly simplified the handling of data. Moreover, this approach has a practical importance, as global parameters (like BOD, COD, and TOC) are usually used to account for organic matter degradation.

The coupling of mass balance equations (derived from the hydrodynamics of the system) with kinetic ones was shown to be an important step in order to adequately describe the actual behavior of the photocatalytic process.

The estimated reaction rate constants increased, while the adsorption ones decreased with the medium salinity.

Among all of the identified intermediates, only three were formed in significant amounts: hydroquinone, catechol, and 3-phenyl-2-propenal, in this order. Catechol formation was severely inhibited by salinity, while 3-phenyl-2-propenal formation was increased by it.

Acute toxicity tests showed that none of the intermediates, at the concentrations in which they were generated in the reaction mixture, presented a higher toxicity than the parent compound (phenol). Therefore, photocatalysis also proved to be quite efficient in removing toxicity, regardless of the salt concentration (up to 50 g L⁻¹).

ACKNOWLEDGMENTS

The authors wish to thank FAPERJ, FUJB, CNPq, and PADCT for financial support and logistics, as well as Degussa for supplying the catalyst.

REFERENCES

- Alemany, L. J., Bañares, M. A., Pardo, E., Martin, F., Galán-Fereres, M., and Blasco, J.M., Photodegradation of phenol in water using silica-supported titania catalysts, *Appl. Catal. B*, 13, 289–297 (1997).
- Al-Rasheed, R., and Cardin, D. J., Photocatalytic degradation of humic acid in saline waters: Part 2. Effects of various photocatalytic materials, *Appl. Catal. A*, 246, 39–48 (2003).
- Augugliaro, V., Palmisano, L., Sclafani, A., Minero, C., and Pelizzetti, E., Photocatalytic degradation of phenol in aqueous titanium-dioxide dispersions, *Toxicol. Environ. Chem.*, 16, 89–109 (1988).
- Azevedo, E. B., Identification and toxicity of generated intermediates during the photocatalytic degradation and Ozonation of phenol in saline medium, D.Sc. Thesis, Universidade Federal do Rio de Janeiro (2003).
- Azevedo, E. B., Aquino Neto, F. R., and Dezotti, M., TiO₂-photocatalyzed degradation of phenol in saline media: lumped kinetics, intermediates, and acute toxicity, *Appl. Catal. B*, 54, 165–173 (2004).
- Baird, C., *Environmental Chemistry*, Freeman, New York (1998).
- Belkacemi, K., Larachi, F., and Sayari, A., Lumped kinetics for solid-catalyzed wet oxidation: a versatile model, *J. Catal.*, 193, 224–237 (2000).

- Bessa, E., Sant'Anna Jr., G. L., Dezotti, M., Photocatalysis: an approach to the treatment of oil field produced waters, *J. Adv. Oxid. Technol.*, 4, 196–202 (1999).
- Bessa, E., Sant'Anna Jr., G. L., Dezotti, M., Photocatalytic/H₂O₂ treatment of oil field produced waters, *Appl. Catal. B: Environ.*, 29, 125–134 (2001).
- Chapra, S. C., and Canale, R. P., *Numerical Methods for Engineers: with programming and software applications*, 3rd ed., McGraw-Hill Book Co., Singapore (1998).
- Czuczwa, J., Leuenberger, C., Tremp, J., and Giger, W., Determination of trace levels of phenol and cresols in rain by continuous liquid-liquid extraction and high-performance liquid chromatography, *J. Chrom. A*, 403, 233–241 (1987).
- D'Oliveira, J.-C., Al-Sayyed, G., and Pichat, P., Photodegradation of 2-chlorophenol and 3-chlorophenol in TiO₂ aqueous suspensions, *Environ. Sci. Technol.*, 24, 990–996 (1990).
- Fogler, H.S., *Elements of Chemical Reaction Engineering*, 3rd ed., Prentice Hall PTR., New Jersey (1999).
- Goldberg, M. C., and Weiner, E. R., Extraction and concentration of phenolic compounds from water and sediment, *Anal. Chim. Acta*, 115, 373–378 (1980).
- Grimes, S. M., and Ngwang, H. C., Methodology for studying oxidation of organic species in solution, *J. AOAC Int.*, 83, 584–587 (2000).
- Hamilton, M. A., Russo, R. C., and Thurston, R. V., Trimmed Spearman-Kärber method for estimating median lethal concentrations in toxicity bioassays, *Environ. Sci. Technol.*, 11, 714–719 (1977).
- Herrmann, J.-M., Heterogeneous photocatalysis: fundamentals and applications to the removal of various types of aqueous pollutants, *Catal. Today*, 53, 115–129 (1999).
- Hoffmann, M. R., Martin, S. T., Choi, W., and Bahnemann, D., Environmental applications of semiconductor photocatalysis, *Chem. Rev.*, 95, 69–96 (1995).
- Ilisz, I., and Dombi, A., Investigation of the photodecomposition of phenol in near-UV-irradiated aqueous TiO₂ suspensions, *Appl. Catal. A*, 180, 35–45 (1999).
- Levenspiel, O., *Engenharia das Reações Químicas*, 1^a ed., Editora Edgar Blücher LTDA., São Paulo (1987).
- Linsebigler, A. L., Lu, G. and Yates Jr., J. T., Photocatalysis on TiO₂ surfaces: principles, mechanisms, and selected results, *Chem. Rev.*, 95, 735–758 (1995).
- Litter, M., Heterogeneous photocatalysis — transition metal ions in photocatalytic systems, *Appl. Catal. B*, 23, 89–114 (1999).
- Mills, A., Davies, R.H. and Worsley, D., Water purification by semiconductor photocatalysis, *Chem. Soc. Rev.*, 22, 417–425 (1993).
- Montgomery, D. C., *Design and Analysis of Experiments*, 3rd ed., John Wiley & Sons Inc., Singapore, (1991).
- Nogueira, R. F. P., Alberici, R. M., Mendes, M. A., Jardim, W. F., and Eberlin, M. N., Photocatalytic degradation of phenol and trichloroethylene: on-line and real-time monitoring via membrane introduction mass spectrometry, *Ind. Eng. Chem. Res.*, 38, 1754–1758 (1999).
- Okamoto, K., Yamamoto, Y., Tanaka, H., Tanaka, M., and Itaya, A., Heterogeneous photocatalytic decomposition of phenol over TiO₂ powder, *Bull. Chem. Soc. Jpn.*, 58, 2015–2022 (1985).
- Peiró, A. M., Ayllón, J. A., Peral, J., and Doménech, X., TiO₂-photocatalyzed degradation of phenol and ortho-substituted phenolic compounds, *Appl. Catal. B*, 30, 359–373 (2001).
- PETROBRAS, Toxic agents acute toxicity determination with *Artemia sp.*, Method N-2588 (1996).
- PETROBRAS, Sample preparation for the toxicity test, Method N-2594 (1996).
- Richard, C., and Boule, P. N., Photocatalytic oxidation of phenolic derivatives: influence of OH[•] and h⁺ on the distribution of products, *New J. Chem.*, 18, 547–552 (1994).
- Santos, F. V., Azevedo, E. B., Sant'Anna Jr., G. L., Dezotti, M., Photocatalysis as a tertiary treatment for petroleum refinery wastewaters, *Braz. J. Chem. Eng.*, 23, 451–460 (2006).
- Serpone, N., Terzian, R., Minero, C., and Pelizzetti, E., *Heterogeneous Photocatalyzed Oxidation*, American Chemical Society, Washington (1993).
- Smith, J. M., *Chemical Engineering Kinetics*, 3rd ed., McGraw-Hill Book Co., Singapore (1981).
- Sobczynski, A., Duczmal, L., and Dobosz, A., Photocatalysis by illuminated titania: oxidation of hydroquinone and p-benzoquinone, *Monatshefte für Chemie*, 130, 377–384 (1999).
- Torres, A. R., Azevedo, E. B., Resende, N. S., Dezotti, M., A comparison between bulk and supported TiO₂ photocatalysts in the degradation of formic acid, *Braz. J. Chem. Eng.*, 24, 185–192 (2007).
- Trillas, M., Pujol, M., and Doménech, X. J., Phenol photodegradation over titanium dioxide, *Chem. Tech. Biotechnol.*, 55, 85–90 (1992).